Study of the intermediate pyrolysis steps and mechanism identification of polymer-derived SiBCN ceramics

Laura Gottardo, Samuel Bernard, Christel Gervais, Markus Weinmann, Philippe Miele

Study of the intermediate pyrolysis steps and mechanism identification of polymer-derived SiBCN ceramics

Laura Gottardo,‡[a] Samuel Bernard,*[a] Christel Gervais,[b] Markus Weinmann[c] and Philippe Miele[a]

The intermediate pyrolysis steps and the mechanisms occurring during the conversion of boron-modified polysilazanes (BmPSs) of the type $[B(C_2H_4SiCH_3NCH_3)_3]_n$ (C_2H_4 = $CHCH_3$, C H $_2CH_2$) into amorphous SiBCN ceramics have been investigated. TGA–DTG experiments coupled with mass spectroscopy and gas chromatography have been applied to investigate the mass loss behaviour during ceramization and to receive information on the nature of the escaping gas species. Solid-state ^{11}B, ^{13}C and ^{29}Si NMR spectroscopy has been applied to probe the local environment of all NMR active nuclei in the precursor, the thermolysis intermediates and the ceramic residue. IR spectroscopy has been performed to receive valuable information on the chemical bonding in all materials. The results contributed (i) to gain structural information on the decomposition process of amorphous SiBCN ceramics during the pyrolytic conversion of processable BmPSs and (ii) to optimize the pyrolytic conversion of BmPSs into SiBCN materials endowed with designed performance properties that surpass those of existing materials. Ceramic conversion starts by the release of methylamine under ammonia atmosphere *via* transamination and disappearance of BC_3 units with the concomitant increased portion of $BC_{3-x}N_x$ ($0 < x < 3$) units in the low temperature regime of the decomposition (RT–200 °C). It is followed by evolution of hydrocarbons due to the cleavage of bonds and formation of radicals that abstract hydrogen. In the high temperature regime of the decomposition, hydrogen is removed due to dehydrocoupling reactions. After heating to 700 °C, BN_3, BCN_2, and SiN_4 domains as well as Si–C–N units of mixed compositions coexist. Further heating to 1000 °C results in a continuous transformation into an amorphous SiBCN network consisting of B(C)N domains, SiC_xN_{4-x} units with $x = 0$, 1, 2 and free carbon.

1 Introduction

The thermal decomposition of preceramic polymers in an oxygen-free atmosphere is an elegant chemical approach for the preparation of *so-called* Polymer-Derived Ceramics (PDCs).[1–7] The chemistry (elemental composition, compositional homogeneity and atomic structure), the processing properties and the reactivity (thermal and chemical) of related polymers can efficiently be controlled and tailored to supply ceramics with the desired elemental composition, structure (amorphous or crystalline), morphology (dense or porous) and shape. It is thus possible to produce ceramics with targeted, improved or even novel properties in a way not possible with other techniques.

Ceramics around the quaternary Si/B/C/N system are a relatively new class of PDCs that exhibit outstanding thermostructural properties.[8–27] Nowadays, they represent the reference in terms of high-temperature stability among non-oxide-type ceramics granting them potential applications in harsh environments as composites,[14] ceramic fibers,[13,17] membranes[18] and ordered porous materials.[20,24]

There are two main single-source polyborosilazane systems that lead to SiBCN ceramics. The first synthetic pathway pioneered by Riedel *et al.* focuses on the synthesis of boron-modified polysilazanes (BmPSs) of the type $[B(C_2H_4SiCH_3NH)_3]_n$.[8] They represent polysilazane rings which are cross-linked *via* –C–B–C– bridges. The second approach proposed by Jansen *et al.* makes use of the synthesis of polyborosilazanes, *i.e.*, polysilazanes cross-linked *via* –B–N–B– bridges.[13] Each of these approaches has its advantages and drawbacks in terms of polymer processing and ceramic properties. BmPSs probably offer better latitude in the tailoring of both their processability (shaping, ceramic yield)

[a]IEM (Institut Europeen des Membranes), UMR 5635 (CNRS-ENSCM-UM2), Universite Montpellier 2, Place E. Bataillon, F-34095, Montpellier, France. E-mail: Samuel.Bernard@iemm. univ-montp2.fr
[b]Laboratoire de Chimie de la Matiere Condensee UMR CNRS 7574, UPMC Univ Paris 06, College de France, 11 place M. Berthelot, 75005 Paris, France
[c]H. C. Starck GmbH, Im Schleeke 78-91, D-38642, Goslar, Germany

‡Present address: EMPA, Laboratory for Advanced Fibers, 5 Lerchenfeldstrasse CH-9014 St. Gallen – Switzerland.

and the properties of the resulting ceramics (microstructure, thermal stability, …) through the design of their chemical composition with respect to the type of functional groups that are bonded to the polymer skeleton. This allowed us to prepare materials for the targeted applications. We therefore focused on this polymer variety and synthesized BmPSs of the type $[B(C_2H_4SiCH_3NCH_3)_3]_n$ (C_2H_4 = $CHCH_3$, CH_2CH_2)[17,20] which offer improved processability compared with their structural analogues $[B(C_2H_4SiRNH)_3]_n$ (R = CH_3,[8,15,24] H,[15] $(NH)_{0.5}$ (ref. 15)). When pyrolyzed in the temperature range 1000–1400 °C, BmPSs lead to amorphous SiBCN ceramics which can combine different functional properties such as extremely high thermal stability, mechanical (creep) stability and electrical conductivity. Subsequent crystallization at 1400–2000 °C gives rise to thermodynamically stable phases, *i.e.*, silicon carbide (SiC), turbostratic B–(C)–N layers encapsulating silicon nitride (Si_3N_4) and "free carbon", depending on the initial composition of the preceramic polymer. In a multi-step preparation process (Fig. 1), we coupled inorganic chemistry and material chemistry to synthesize BmPSs of the type $[B(C_2H_4SiCH_3NCH_3)_3]_n$ (C_2H_4 = $CHCH_3$, CH_2CH_2) with favourable processing properties which are ideal precursors of specifically shaped SiBCN materials such as mesoporous ceramics, ceramic fibers and hollow fiber membranes.

In general, the preparation of shaped materials is closely dependant on the rheology of the preceramic polymers.[28] Furthermore, volume shrinkage and therefore shape retention during the polymer-to-ceramic conversion is intimately linked to the chemistry of the polymers including the structural rearrangements on an atomic scale.[29] In particular, the chemistry involved during the polymer-to-ceramic conversion includes a complex sequence of structural and chemical changes based on molecular rearrangements and the release of gaseous by-products which are inherently related to the molecular structure and chemistry of preceramic polymers. Therefore, it is particularly essential to control as much as possible thermally induced molecular rearrangements by carefully adjusting the molecular structure of preceramic polymers.

In BmPSs of the type $[B(C_2H_4SiRNH)_3]_n$ (R = H, CH_3, $(NH)_{0.5}$), the influence of the polymer architecture on the structure of the final ceramic has been investigated in detail by solid-state NMR spectroscopy.[30–32] Based on these results, conclusive pyrolysis mechanisms were suggested which allowed for an optimization of various properties and especially the thermal stability of SiBCN ceramics. Until now, no efforts have been made to explore the mechanism of the polymer-to-ceramic conversion of their processable analogs with NCH_3 units, *i.e.*, BmPS of the type $[B(C_2H_4SiCH_3NCH_3)_3]_n$ (C_2H_4 = $CHCH_3$, CH_2CH_2), in particular, by solid-state NMR coupled with GC/MS and FTIR, as those described in this article.

Herein, a systematic mechanistic study of the polymer-to-ceramic conversion of $[B(C_2H_4SiCH_3NCH_3)_3]_n$ in ammonia and/or nitrogen atmosphere is performed. The individual chemical processing steps and the related structural and chemical changes occurring during the polymer-to-ceramic conversion are investigated in detail using a combination of *in situ* thermoanalytical experiments coupled with gas chromatography and mass spectrometry, and *ex situ* solid-state NMR and FT-IR spectroscopy. On the basis of the structural assignment, pyrolytic decomposition pathways are outlined.

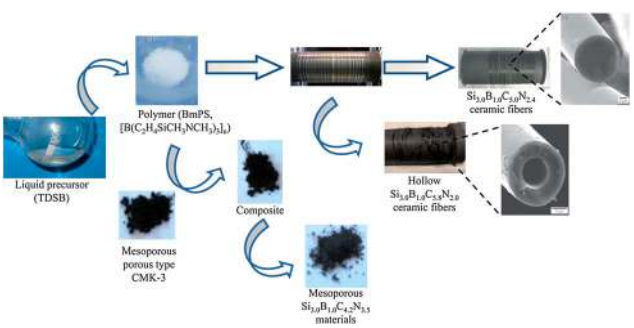

Fig. 1 Overall synthetic path employed to generate fibers and mesoporous SiBCN materials from BmPSs of the type $[B(C_2H_4SiCH_3NCH_3)_3]_n$ (C_2H_4 = $CHCH_3$, CH_2CH_2).

2 Experimental section

2.1. General comment

All synthesis reactions have been carried out in a purified argon atmosphere passing through successive columns of BTS-catalyst and phosphorus pentoxide by means of standard Schlenk manipulations and vacuum/argon-line techniques. Dichloromethylvinylsilane (DMVS, $CH_2{=}CHSiCH_3Cl_2$) was obtained from Sigma-Aldrich and freshly distilled from magnesium. Borane dimethylsulfide $BH_3S(CH_3)_2$ (2 M solution in toluene) was obtained from Sigma-Aldrich and used without further purification. Methylamine (MA), anhydrous (Sigma-Aldrich, 99+%), was used as-received. Extra dry tetrahydrofuran (THF, 99.5%) and toluene (99.85%) over molecular sieves (Aeroseal®) were obtained from AcrosOrganics. Manipulation of the chemical products was made inside an argon-filled glove box (Jacomex BS521) dried with phosphorus pentoxide.

2.2. Sample characterization

Characterization was conducted on **BmPS*RT*** powders which were previously milled then sieved into microparticles with size ≤ 80 μm.

Thermogravimetric analysis (TGA) of the polymer-to-ceramic conversion was recorded on a Setaram TGA 92 16.18. After introduction of **BmPS*RT*** under argon, the tube was pumped under vacuum and refilled with the desired gas used as the atmosphere. The heating program was similar to that used for thermolysis (*c.f.* 2.4). *ca.* 40 mg of the sample were investigated at ambient atmospheric pressure using silica crucibles. Experiments were also performed in ammonia as well as in nitrogen atmosphere at 1 °C min^{-1} from RT to 1000 °C. Experimental differential thermogravimetric (DTG) data were generated from TGA measurements, and then simulated using the multi-peak fitting Lorentz distribution.[33] Gas chromatography coupled with mass spectrometry (GC/MS) has additionally been recorded during TG experiments using nitrogen purging gas according to the sensitivity of GC columns with ammonia. They were conducted on **BmPS*RT*** and **BmPS*200*** (polymer cross-linked under ammonia at 200 °C) in flowing nitrogen in a continuous process. The gas stream was analyzed with a portable micro-chromatograph μGC M200 from the Agilent M Series coupled with a mass

spectrometer detector. The μGC/MSD is commercialized by S.R.A. Instruments. The μGC is composed of 2 columns and 2 micro-thermal conductivity detectors (μ-TCD). Hydrogen was separated on a molecular sieve column (12 m × 0.32 mm, 5 Å) and quantified with the TCD detector after the calibration of the μGC with a standard containing hydrogen at 2093 ppm in nitrogen. The presence of other gases such as methane, ammonia or methylamine was checked on the OV1 column (10 m × 0.15 mm i.d.), the identification being realized by its coupling with an Agilent quadruple mass spectrometer detector (MSD 5973). The spectra of each detected compound were compared with those of the spectral library. SCAN and SIM were chosen in order to have a maximum of information about the emitted gases. For the SIM mode, 3 ions have been selected: 16, 17 and 30. The OV1 and molecular sieve column temperatures were fixed at 90 °C, while the injection time was fixed to 250 and 200 ms respectively; the head column pressure was fixed at 27.6 psi for the molecular sieve column and 30.7 psi for the OV1 column. Argon was used as the carrier gas for the separation and quantification of hydrogen, and helium as the carrier gas when the OV1 column was employed. IR and ^{11}B, ^{13}C and ^{29}Si solid-state NMR spectra of **BmPS*RT*** and its heat-treated samples isolated at different intermediate temperatures in the range of 100 to 1000 °C (labeled **BmPS*T***, with *T* being the intermediate temperature) were analyzed at RT. Fourier transform infrared spectra (FT-IR) of samples **BmPS*RT* → *700*** were obtained from a Nicolet Magna 550 Fourier transform-infrared spectrometer in a KBr matrix (dried at 120 °C in air). It should be mentioned that infrared spectroscopy measurements of the sample **BmPS*1000*** were performed using a Nicolet 380 FT-IR spectrometer coupled with the Attenuated Total Reflectance (ATR) accessory. ^{1}H and ^{13}C NMR spectra of a polymer in $CDCl_3$ were obtained using a Bruker AM 300 spectrometer operating at 300 MHz and 62.5 MHz, respectively. Solid-state ^{11}B MAS NMR spectra were recorded at 11.75 T on a Bruker Avance 500 wide-bore spectrometer operating at 160.49 MHz, using a Bruker 4 mm probe and a spinning frequency of the rotor of 14 kHz. The spectra were acquired using a spin-echo $\theta-\tau-2\theta$ pulse sequence with $\theta = 90°$. The τ delay was synchronized with the spinning frequency and a recycle delay of 1s was used. Solid-state ^{13}C and ^{29}Si CP MAS NMR spectra were recorded at 75.51 and 59.66 MHz, respectively on a Bruker Avance 300 spectrometer (7 T) using 7 mm Bruker probes and spinning frequencies of 5 kHz. CP MAS experiments were performed under the following Hartmann–Hahn match condition: both RF channel levels, $\omega_{1S}/2\pi$ and $\omega_{1I}/2\pi$, were set at about 50 kHz. A ^{29}Si MAS spectrum was also recorded for **BmPS*1000*** with a recycle delay of 60s to ensure full relaxation of the spins. Chemical shift values are reported relative to tetramethylsilane for ^{1}H, ^{13}C and ^{29}Si ($\delta = 0$) or BF_3OEt_2 for ^{11}B. The spectra were simulated with the DMFIT program.[34]

2.3. Synthesis

$[B(C_2H_4SiCH_3NCH_3)_3]_n$ has been synthesized by hydroboration of DMVS according to procedures described in the literature[35–37] and subsequent aminolysis of the tris(dichlorosilylethyl)borane (TDSB)[17,19–21] with methylamine (MA) in THF at 0 °C (Fig. 2).

40.6 ml (1307.3 mmol) of MA were trapped in a Schlenk tube cooled with liquid nitrogen. 63.3 g (144.8 mmol) of TDSB were

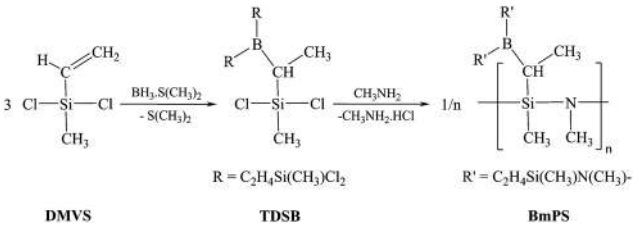

Fig. 2 Synthetic pathway applied for the synthesis of $[B(C_2H_4SiCH_3NCH_3)_3]_n$ (BmPS; $C_2H_4 = CHCH_3$, CH_2CH_2).

introduced into a Schlenk flask equipped with a condenser and dissolved in 700 ml of THF. The Schlenk tube containing MA was connected to the cooled Schlenk flask containing the THF solution of TDSB and removed from the liquid air cooling bath. Both parts were linked *via* an interconnection flexible tube which was evacuated and subsequently filled with argon. Argon was slowly introduced into the Schlenk tube and MA passed through the vigorously stirred TDSB solution which was cooled to 0 °C. When addition was finished, the stirred mixture was allowed to warm to room temperature (RT) and kept at this temperature overnight. Removal of the couple product methylamine hydrochloride from the polymer solution was performed through a pad of Celite. The solvent was removed by distillation (RT/1.5 × 10^{-1} mbar) *via* an ether bridge to release a colorless powder labeled **BmPS*RT*** (42.1 g) which is sensitive to oxygen and moisture and thus has to be manipulated in an inert atmosphere.

Anal. found (wt%): C, 40.81; H, 11.6; N, 15.43; B, 3.51; Si, 25.7; O, 0.68. $[Si_{3.0}B_{1.1}C_{11.8}N_{3.6}H_{37.7}]_n$ ([326.3]$_n$) Calcd C, 46.25; H, 9.70; N, 13.54; B, 3.42; Si, 27.04. $[Si_{3.0}B_{1.0}C_{12.0}N_{3.0}H_{30.0}]_n$ IR (KBr/cm^{-1}): ν (N–H) = 3427, 3320, 3229 w; ν (C–H) = 2953 s, 2895 s, 2805 m; δ(N(H)CH$_3$) = 1599 w; δasym(CH$_3$) = 1462 w; ν(C–C) = 1355 w; δ(Si–CH$_3$) = 1257 s; δ(C–B–C) = 1181 m; δ(SiCH$_2$C) = 1139 m; ν(C–N) = 1061 m; δ (N–Si–N) = 912 sh-876 *vs.* ^{1}H NMR ($CDCl_3$) (ppm): $\delta = 0.10$ (br, SiC*H*$_3$), $\delta = 0.21$ (vbr, SiC*H*$_2$CH$_2$B), $\delta = 0.80$ (br, C*H*$_3$CHBSi), $\delta = 1.10$ (br, SiCH$_2$C*H*$_2$B), $\delta = 1.23$ (br, CH$_3$C*H*BSi), $\delta = 2.30$ (vbr, NC*H*$_3$).

2.4. Thermolysis

For each thermolysis experiment, **BmPS*RT*** is introduced into a nitrogen-filled glove box connected to a horizontal tube furnace (Nabertherm type RS 80/500/11, Germany). Samples of typically 2 g are filled into an alumina boat and then introduced into the furnace. The tube is evacuated (10^{-3} mbar) and refilled with ammonia (99.995%). Subsequently, samples are subjected to a cycle of ramping of 0.5 °C min^{-1} to 200 °C, dwelling there for 1 h in flowing ammonia (200 mL min^{-1}). Ammonia supply is stopped, nitrogen is introduced in the furnace and the samples are held for 1 h at 200 °C. Samples are subsequently heated to 1000 °C (1 °C min^{-1}) and annealed at this temperature for 2 h in flowing nitrogen (200 mL min^{-1}). Samples are finally cooled to RT at 5 °C min^{-1}.

3 Results and discussion

In the present study, we discuss the polymer-to-ceramic conversion of $[B(C_2H_4SiCH_3NCH_3)_3]_n$ ($C_2H_4 = CHCH_3$, CH_2CH_2) labeled **BmPS*RT*** in the temperature range from RT to

1000 °C which covers the amorphous intermediate stages leading to SiBCN ceramics.

3.1. Ceramic conversion in flowing nitrogen

Weight losses and decomposition rates (Differential Thermogravimetric (DTG) data) were first monitored during thermal decomposition of **BmPS*RT*** by TGA in flowing nitrogen up to 1000 °C (1 °C min^{-1}). The result is shown in Fig. 3.

Thermal degradation under nitrogen occurs through a continuous single-step weight loss from 80 °C up to 550 °C providing a black residue. The weight loss after thermolysis at 1000 °C measures *ca.* 90 wt%. The associated DTG curve distinguishes several decomposition steps. The plotted curve is characterized by one temperature T_{max} = 250 °C at which the decomposition rate is maximum, but the presence of smaller peaks and the broadening and asymmetry of some peaks due to peak overlapping suggest a more complicated decomposition process. The latter is made of at least eight mechanisms as marked on the DTG curve after a deconvolution using the Lorentz multi-peak function which has been reported to be the best appropriate fitting method for TG experiment modelisation.[33]

Here, we coupled TG experiments with GC/MS and we observed gaseous species with m/z = 101 which may correspond to the monomeric fragment $[C_2H_4SiCH_3NHCH_3]^+$. Moreover, by-products with m/z = 56 and 57 were released. The identification of relatively high m/z indicates depolymerization of the polymer. This is probably a consequence of the low degree of cross-linking and the lack of potential cross-linking sites such as SiH, NH, $SiCH{=}CH_2$ in the polymer network which are prerequisites for avoiding depolymerization and volatilization of low-molecular weight species and therefore obtaining high ceramic yields. N(H)groups present in **BmPS*RT*** have a lower capability to self-condense in comparison to NH_2 groups present in $[B(C_2H_4SiCH_3NH)_3]_n$ which displays a ceramic yield in the range of 54 to 62 wt%[8,15,24] depending on the atmosphere and the synthetic pathway applied. In addition elimination of species with lower m/z ratio was observed in the temperature range of 80–650 °C, *i.e.*, fragments with m/z = 2 (H_2), 15, 16 (CH_4), 26 (C_2H_2), 30 and 31 (CH_3NH_2) (Fig. 4). The majority of these species are observed in BmPSs of the type

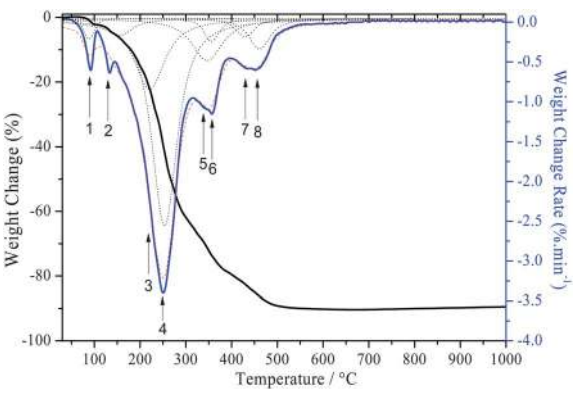

Fig. 3 TGA–DTG curves of **BmPS*RT*** decomposed in flowing nitrogen at 1 °C min^{-1} up to 1000 °C.

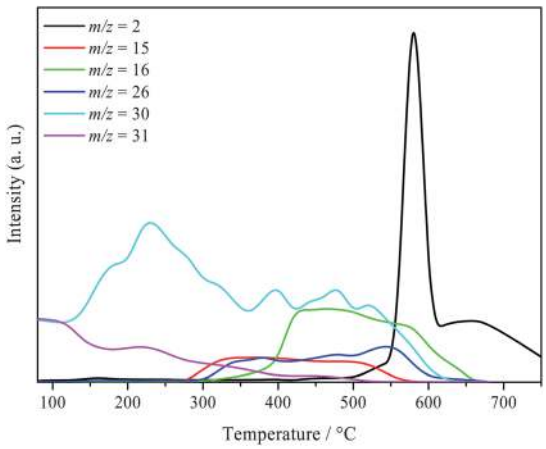

Fig. 4 GC/MS profiles of **BmPS*RT*** decomposed in flowing nitrogen at 1 °C min^{-1} up to 1000 °C.

$[B(C_2H_4SiCH_3NH)_3]_x[NH]_{3-x}$ ($1 \leq x \leq 3$).[32] However, in our case, we can identify fragments at m/z = 30 and 31 which are not observed in these systems whereas the fragment at m/z = 28 attributed to C_2H_4 is not observed.

The release of methylamine mainly occurs in the low temperature regime of the thermal decomposition. It probably arises from the condensation of terminal $N(H)CH_3$ groups present in **BmPS*RT***. The identification of hydrocarbons, mainly at intermediate temperatures, indicates cleavage of Si–C and C–H bonds, leading to the formation of radicals that further abstract hydrogen. Hydrogen release is known to be caused by dehydrocoupling reactions at higher temperatures.[38] As a consequence of the depolymerization during thermolysis, it is not possible to maintain the shape of the green part and to generate SiBCN materials from **BmPS*RT*** in the desired form. As an illustration, the integrity of green fibers that can be spun from this precursor using melt-spinning[17] cannot be preserved and hollow ceramic fibers with a dense shell are thus obtained (Fig. 1).

We believe that the formation process consists of the following steps: up to 250 °C, the core of the green fiber is gradually depolymerized and evaporated, while the surface is cross-linked *via* condensation of terminating $NHCH_3$ groups. In a second step above 250 °C, the subsequent solid-state decomposition leads to the release of hydrocarbons and dehydrogenation, releasing the hollow ceramic fibers with an empirical formula of $Si_{3.0}B_{1.0}C_{5.8}N_{2.0}$.

Depolymerization can be avoided by increasing the cross-linking density (*i*) of the native polymer through introduction of reactive groups such as SiH, $SiCH{=}CH_2$ or NH that provide latent reactivity (strategy 1) and/or (*ii*) by a pre-pyrolysis treatment in a reactive atmosphere during the low temperature process of the ceramic conversion, *i.e.*, curing (strategy 2). The first strategy is usually made to the detriment of the processability of the considered polymer for the further shaping process. To retain the elastic and rheological properties of $[B(C_2H_4SiCH_3NCH_3)_3]_n$, the second strategy was thus the preferred option.

Several concepts have been developed for curing processes. They are mainly based on surface hardening by oxidation in air

or electron beam irradiation.[39,40] Cross-linking by ammonia has been considered as a promising method for the curing of preceramic polymers containing alkylamino groups.[41] The introduction of definite and adjustable amounts of nitrogen into the polymer *via* ammonia treatment, *i.e.*, thermal cross-linking at low temperature, is expected to avoid depolymerization during the further pyrolysis.

3.2. Thermal cross-linking of $[B(C_2H_4SiCH_3NCH_3)_3]_n$ with ammonia

TGA of **BmPS*RT*** in flowing ammonia was performed in the temperature range of RT–1000 °C at a heating rate of 1 °C min^{-1} (Fig. 5) to determine the optimum temperature range required for cross-linking of **BmPS*RT***.

BmPS*RT* undergoes a continuous weight loss of *ca.* 82.7% in the temperature range from 50 to 600 °C. The ceramic yield after thermolysis at 1000 °C of *ca.* 17.3% is higher than that measured under nitrogen (*ca.* 10.5%) using similar heating conditions. Ammonia is known to remove carbon-based organic groups from preceramic polymers by diffusion-type mechanisms.[33] Therefore, weight loss measured under ammonia in comparison to nitrogen is usually higher.[33a] Here, this points to the fact that volatilization of fragments occurring under nitrogen is probably inhibited if ammonia is used. The residue is a lightly gray colored powder confirming that free carbon in the final material has been eliminated. Differential TGA suggests a two-step decomposition process; the first step appears from 50 to 200 °C ($\Delta m/m_0 \sim 18.3$ wt%) followed by the second step which is observed between 200 to 650 °C ($\Delta m/m_0 \sim 64.4$ wt%).

In comparison with TGA performed in a nitrogen atmosphere (Fig. 3), the weight loss recorded in the temperature range of 50–200 °C in flowing ammonia is associated with an additional process (three DTG peaks after deconvolution, Fig. 5). Furthermore, the weight loss measured at 200 °C (*ca.* 18.3 wt%) is higher if using ammonia than the weight loss measured at 200 °C under nitrogen (*ca.* 12 wt%). In contrast, the weight loss in the second decomposition step which occurs from 200 to 650 °C is much lower if pyrolysis is performed in an ammonia atmosphere (*ca.* 64.4 wt%) compared with that measured (200–550 °C) under nitrogen (*ca.* 78 wt%). Accordingly, the reaction of ammonia with **BmPS*RT*** occurs predominantly in the low temperature regime of the polymer-to-ceramic conversion.

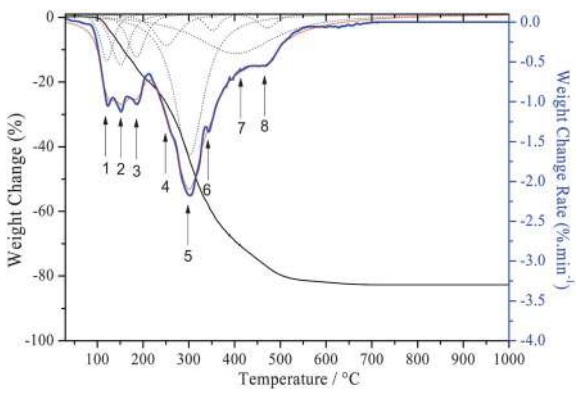

Fig. 5 TGA–DTG curves of **BmPS*RT*** in flowing ammonia at 1 °C min^{-1} up to 1000 °C.

To support our discussion, we have investigated thermomechanical analysis (TMA) under nitrogen on **BmPS*RT*** and **BmPS*200***, *i.e.*, the sample heat-treated at 200 °C under ammonia (see ESI, Fig. S1†) as pellets (5 mm in diameter and ~1 mm in thickness). **BmPS*RT*** exhibits a significant dimensional change of >90% under compressive load (0.9 N) upon heating to 200 °C indicating its fusibility and thus its potential for fiber spinning.[17] In contrast, **BmPS*200*** is almost stable under compressive load in the considered temperature range. Curing at 200 °C of **BmPS*RT*** in an ammonia atmosphere thus converts the processable precursor into an almost infusible cross-linked preceramic network, which usually is mandatory for hardening low-dimensional shapes such as (nano)fibers, porous material in order to retain shape integrity during thermolysis. In comparison, the sample heat-treated at 200 °C under nitrogen (**BmPS*200N₂***) is not stable under compressive load since it exhibits a major dimensional change (*see* Fig. S1†). Based on these observations, we performed the curing process between 25 and 200 °C in an ammonia atmosphere prior to pyrolysis under nitrogen up to 1000 °C. A dwelling time of 2 h (1 h under ammonia and 1 h under nitrogen) was fixed at 200 °C.

The combination of a low-temperature treatment, *i.e.*, curing, of **BmPS*RT*** in ammonia (0.5 °C min^{-1} from RT to 200 °C) and thermolysis in a nitrogen atmosphere at a heating rate of 1 °C min^{-1} (200 °C to 1000 °C) allowed us to modify the following characteristic:

(1) It increased the ceramic yield by ~28%, as evident from a comparison of Fig. 6 with Fig. 3.

(2) It allowed maintaining the shape imposed during the polymer processing. For example, dense ceramic fibers with an empirical formula of $Si_{3.0}B_{1.0}C_{5.0}N_{2.4}$ have thus been produced (Fig. 1).

A comparison of the chemical composition of fibers produced under nitrogen ($Si_{3.0}B_{1.0}C_{5.8}N_{2.0}$) with those obtained with NH_3 pre-treatment ($Si_{3.0}B_{1.0}C_{5.0}N_{2.4}$) clearly indicated that not only nitrogen is introduced by the additional cross-linking in ammonia but that additionally carbon is removed.

To well understand the beneficial effect of a curing under ammonia, we combined TG experiments with gas chromatography coupled with mass spectrometry (GC/MS). However, the identification of gaseous species evolving during the curing

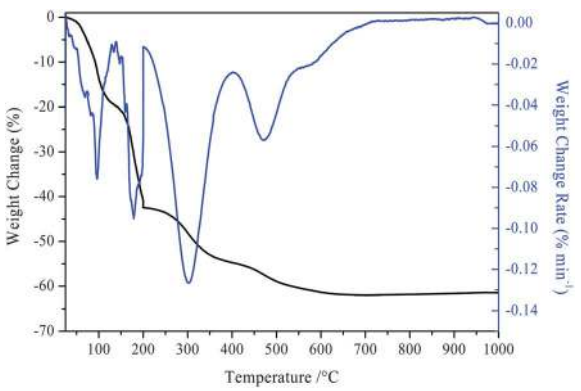

Fig. 6 TGA–DTG curves of **BmPS*RT*** in flowing ammonia up to 200 °C at 0.5 °C min^{-1} followed by thermolysis in nitrogen from 200 to 1000 °C at 1 °C min^{-1}.

process by TG/MS was not possible in the temperature range of RT → 200 °C due to the use of ammonia. TG under nitrogen coupled with GC/MS has been performed in the temperature range of 200–1000 °C. The results are shown in Fig. 7.

The nature and proportion of the gaseous by-products that evolve during the pyrolysis of **BmPS*200*** under nitrogen from 200 to 1000 °C are similar to those of **BmPS*RT*** pyrolyzed in a nitrogen atmosphere. However, a major amount of ammonia is identified around 250 °C which probably results from the presence of NH or NH_2-containing groups in the molecular structure. Based on the TGA/MS results we distinguish three temperature domains during the decomposition of **BmPS*RT***:

(1) RT → 200 °C.
(2) 200 °C → 450 °C.
(3) 450 °C → 1000 °C.

So far, no comprehensive studies have been undertaken on the pyrolysis behavior of boron-modified polysilazanes of the type $[B(C_2H_4SiRNR)_3]_n$ in an ammonia atmosphere, whereas only few exist for polycarbosilanes and polycarbosilazanes.[38,42,43]

Mutin *et al.*[38] showed that Si–H and $Si–CH_3$ as well as $Si–CH_2–Si$ units in polycarbosilane are easily modified by ammonia according to eqn (1). This mechanism is quite favored by polymers containing Si–H units which are sensitive to nucleophilic substitution.

$$\equiv Si–R + NH_3\ (g) \rightarrow \equiv Si–NH_2 + RH\ (R = H, CH_3, CH_2–Si\equiv) \quad (1)$$

Homolytic cleavages probably occur in a parallel way according to eqn (2)–(4).

$$\equiv Si–R \rightarrow \equiv Si^{\cdot} + R^{\cdot}\ (R = H, CH_3, CH_2–Si\equiv) \quad (2)$$

$$R^{\cdot} + NH_3\ (g) \rightarrow RH + {}^{\cdot}NH_2 \quad (3)$$

$$\equiv Si^{\cdot} + {}^{\cdot}NH_2 \rightarrow \equiv SiNH_2 \quad (4)$$

Such mechanisms have also been proposed by Interrante *et al.* for vinyl-substituted polysilanes,[42] and by Mutin *et al.* for polysilazanes.[43] They probably occur below 500 °C.

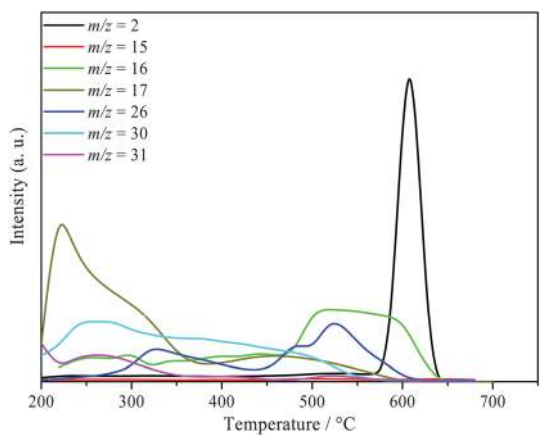

Fig. 7 GC/MS profiles for **BmPS*RT*** decomposed in flowing ammonia up to 200 °C at 0.5 °C min^{-1} followed by thermolysis in nitrogen from 200 to 1000 °C at 1 °C min^{-1}.

In the presence of N–Me groups in the preceramic network, *e.g.* in *N*-methyl polysilazanes,[43] release of methylamine is detected around 450 °C. It arises from the substitution of NCH_3 groups by ammonia, *i.e.*, a trans-amination according to eqn (5) and (6).

$$\equiv Si–NCH_3–Si\equiv + NH_3\ (g) \rightarrow \equiv Si–NH_2 + \equiv Si–NCH_3H \quad (5)$$

$$\equiv Si–NHCH_3 + NH_3\ (g) \rightarrow \equiv Si–NH_2 + CH_3NH_2 \quad (6)$$

Si–NMe–Si units are thus cleaved by formation of $Si–NH_2$ and Si–NMeH entities. The latter are subsequently transformed into $SiNH_2$ and $MeNH_2$ which is released. $Si–NH_2$ groups condense with formation of Si–NH–Si and $N(Si)_3$ units by release of ammonia according to eqn (7) and (8).

$$\equiv Si–NH_2 + \equiv Si–NH_2 \rightarrow \equiv Si–NH–Si\equiv + NH_3 \quad (7)$$

$$\equiv Si–NH–Si\equiv + \equiv Si–NH_2 \rightarrow =N(Si)_3 + NH_3 \quad (8)$$

In $[B(C_2H_4SiCH_3NCH_3)_3]_n$, most probably trans-amination reactions of either internal $Si–NCH_3–Si$ units as depicted in eqn (5) and (6) or terminal $Si–NHCH_3$ units occur during the curing process under ammonia, thereby releasing methylamine. As-formed $Si–NH_2$ units self-condense during further heat treatment to release ammonia according to eqn (7) and (8). Therefore, the release of ammonia at intermediate temperatures is a consequence of condensation reactions that occur during the curing process finally leading to the formation $N(Si)_3$ units. Besides, we cannot exclude the possibility of an ammonolysis of $SiCH_3$ groups according to eqn (1)–(4) resulting in the elimination of methane and the formation of cross-linking Si–NH–Si units. To discuss on these mechanisms, ^{11}B, ^{13}C and ^{29}Si solid-state NMR and FT-IR spectroscopies have been used to explore the structural changes of **BmPS*RT*** that occur during its conversion into ceramics in ammonia (200 °C) and nitrogen atmospheres (200–1000 °C).

3.3. Structural design of the intermediate steps leading to the ceramic networks

After having fixed appropriate conditions for curing under ammonia, the identification of the relevant chemical reactions was performed based on the chemistry and structure of the polymer using FT-IR and solid-state NMR spectroscopy. Such techniques allow for the determination of chemical structures of the intermediate solid phase material present after the individual decomposition steps identified by TGA–GC/MS.

Representative FT-IR spectra of **BmPS*RT*** and its pyrolysis products obtained in the temperature range of 100–1000 °C are given in Fig. 8.

The IR spectrum of **BmPS*RT*** shows the characteristic stretching and deformation bands of all expected motifs. The series of weak absorption signals for the N–H stretching modes in the 3229–3427 cm^{-1} region demonstrate the presence of $NHCH_3$ ending groups in the polymer structure. Strong and very broad aliphatic C–H bands are also observed in the 2800−2951 cm^{-1} range. In particular, N-bonded C–H (ν(NC–H) = 2805 cm^{-1}) and Si-bonded C–H (ν(SiC–H) = 2953 cm^{-1} and 2895 cm^{-1}) vibrations can be differentiated. There is a band

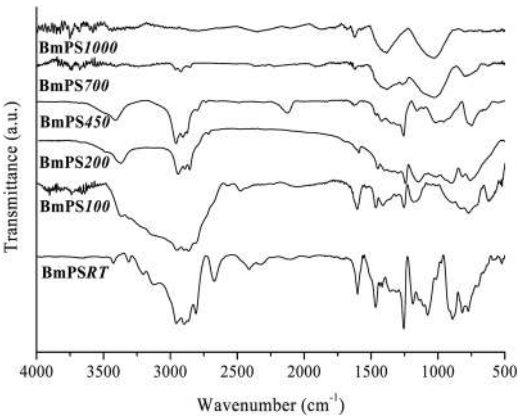

Fig. 8 FT-IR spectra of **BmPS*RT*** and **BmPS*T* (*T*: 100 → 1000)** after heat-treatment in flowing ammonia up to 200 °C at 0.5 °C min^{-1} and subsequent heating in flowing nitrogen from 200 to 1000 °C at 1 °C min^{-1}.

emerging at ~2700 cm^{-1} which is complex to attribute. Such a band is systematically present when using methylamine as the linking agent.[30] It could be assigned to methylamine borane-based complexes. However, even though our proposition is in complete agreement with solid-state NMR (*see later*), there is a lack of evidence or discussion in the literature to support our contentment with regard to this attribution. The band assigned to N–H bond deformation in $NHCH_3$ ending groups is located at 1599 cm^{-1} whereas those which are assigned to the deformation of CH_3 groups are located at 1462 cm^{-1}. The band attributed to Si–CH_3 group deformation appears at 1257 cm^{-1} and a broad N–Si–N asymmetric stretching at 876–912 cm^{-1} as well as δ(C–B–C) at 1181 cm^{-1} are observed. The latter, common in the family of BmPSs, indicates a trigonal planar coordination of boron by three carbon atoms due to α- and/or β-hydroboration reactions. The assigned major absorptions in the infrared spectrum are compiled in the Experimental section. IR spectra of samples isolated below 200 °C (**BmPS*100*** and **BmPS*200***) appear significantly changed in comparison with those of **BmPS*RT*** after ammonia treatment. The cross-linking with ammonia involves the reduction in intensity of bands around 1080 cm^{-1} (ν (C–N)) and 1586 cm^{-1} (N–H deformation in –N(H)CH_3 groups) and a modification of the IR profile in the 2600–3500 cm^{-1} range suggesting the loss of internal $(Si)_2NCH_3$ and terminal (Si)N(H)CH_3 groups. In particular, the series of bands in the range of 3000–3500 cm^{-1} attributed to vibrations of N–H bonds of terminal N(H)CH_3 groups disappear confirming evolution of methylamine during curing under ammonia as suggested on the basis of TGA-GC/MS (eqn (5) and (6)). The appearance of an absorption band centered at 3425 cm^{-1} assigned to the stretching of N–H bonds as well as the gradual decrease of ν_{C-H} absorption bands reflects the substitution of $(Si)_2NCH_3$/SiN(H)CH_3 groups with $SiNH_2$ units. The latter condense to form Si–NH–Si and finally $N(Si)_3$ linkings according to eqn (7) and (8), respectively. These results nicely mirror the findings of the TGA–GC/MS investigations described above. The deformation vibration of the silicon-bonded methyl group at 1254 cm^{-1} is present even after thermolysis at 200 °C, indicating that reactions involving Si–C or C–H cleavage caused by an ammonolysis of $SiCH_3$ groups with ammonia are limited in this temperature range. Others bands such as δ (C–B–C) at 1181 cm^{-1} observed in **BmPS*RT*** almost disappeared after heat-treatment at 200 °C.

The IR spectra of the sample exposed to higher temperatures (**BmPS*450*** and **BmPS*700***) display a band that appears at 2105 cm^{-1}; it corresponds to Si–H vibrations. Such Si–H units most probably form by the cleavage of the Si–C bonds, *e.g.* from the Si–C_2H_4–B units, through a radical reaction thereby forming Si˙ and ˙C_2H_4–B radicals as exemplarily reported in eqn (2) and subsequent hydrogen abstraction from ˙C_2H_4–B, finally releasing Si–H and –CH_2=CHB moieties. The latter readily decomposes at elevated temperatures with formation of B–N bonds (1460 cm^{-1} and 750 cm^{-1}) and Si–C units (800–1000 cm^{-1}) or free carbon whereas Si–H is subject to dehydrocoupling reactions with NH units thereby forming Si–N units, as supported by the identification of molecular hydrogen by GC/MS (eqn (9)).

$$\equiv Si–H + =N–H \rightarrow \equiv Si–N= + H_2 \quad (9)$$

The IR spectra of the pyrolysis intermediates calcined at 700 °C (**BmPS*700***) and 1000 °C (**BmPS*1000***) clearly display major changes in the range of 2805–2953 cm^{-1}, indicating the disappearance of ν_{C-H} vibrations and accordingly elimination of residual hydrogen from the precursors. These findings point out the fact that the transformation of the original polymer into an amorphous network is completed at 1000 °C. At 1000 °C, we can identify broad bands indicating the predominantly amorphous state of the materials, which contain a variety of elemental bonds (such as Si–C, Si–N (800–1250 cm^{-1}), B–N (1300–1600 cm^{-1})) with a distribution of bond lengths and angles that cause a lack of long-range order.

Multinuclear solid-state NMR spectroscopy is another tool which is extremely helpful to structurally investigate the pyrolysis intermediates in order to receive valuable information on atomic rearrangements during the polymer-to-ceramic transformation by probing the local environment of various NMR-active nuclei.

Such investigations of the ceramic conversion of molecular precursors have as a matter of routine been performed for Si- and B-based non-oxide ceramics including Si/C,[44] Si/C/N,[45,46] Si/B/C/N[24,30–32,47] and B/N[48] systems. However, BmPSs of the type $[B(C_2H_4SiRNR')_3]_n$ have only been investigated for R′ = H (R = CH_3, H),[24,30,32] whereas those with R′ = CH_3, which display very different pyrolysis mechanisms, have not been studied so far. Here, we try to give a detailed picture of the decomposition process of BmPSs of the type $[B(C_2H_4SiCH_3NCH_3)_3]_n$ during their ceramic conversion up to 1000 °C under ammonia (200 °C) and nitrogen (200–1000 °C), based on ^{29}Si, ^{11}B and ^{13}C solid state NMR spectroscopy.

^{11}B, ^{13}C and ^{29}Si isotopes are sufficiently abundant to record the respective NMR spectra without isotopic enrichment. Nevertheless, ^{13}C and ^{29}Si spectra were recorded using the cross-polarization (CP) technique to obtain spectra with a reasonable signal-to-noise (*S*/*N*) ratio. The lack of protons in the sample heat-treated at 1000 °C prevented the use of CP and thus a single pulse ^{29}Si MAS of **BmPS*1000*** was recorded. It should be noted that ^{29}Si and ^{13}C CP MAS spectra of **BmPS*100*** were compared with the corresponding single pulse ^{29}Si and ^{13}C MAS (*see* ESI, Fig. S2†) and similar signals were observed with a better signal to noise ratio when using *cross*-polarization which suggests that CP spectra are fairly quantitative.

Experimental ^{11}B MAS NMR spectra recorded at 11.75 T are shown in Fig. 9. Since ^{11}B is a quadrupolar nucleus with $I = 3/2$, the isotropic value of its chemical shift does not correspond to the barycentre of the resonance signal, which is dominated by the second-order quadrupolar broadening.[49] According to the idealized structure of $[B(C_2H_4SiCH_3NCH_3)_3]_n$ (*cf.* Fig. 2), the presence of BC_3-coordination environments, *i.e.*, tri-coordinated boron, is expected. However, the experimental spectrum reflects a large heterogeneity in the local chemical environment of the boron nuclei: both distorted tetrahedral and trigonal coordinations are identified. In particular, the ^{11}B NMR spectrum of the **BmPS*RT*** exhibits relatively broad and overlapping signals between 70 and 10 ppm and a sharp resonance centered at −10 ppm. These are common structural features observed in BmPSs, referring to distorted trigonal BX_3 ($\delta_{iso}(^{11}B)$ at 76.5 and 45.8 ppm and C_Q values of 4.2 and 4.3 MHz respectively) and tetra-coordinated BX_4 sites, respectively.[31,32] Based on the chemical shift values, the tri-coordinated boron atoms, *i.e.*, BX_3, can be assigned to BC_3 and, to a minor extend BC_2N and/or BCN_2 environments. A precise determination of the local environment of the tetra-coordinated boron atoms is not possible, but the chemical shift value suggests that boron is not bonded to hydrogen atoms. Considering the synthesis, the formation of BX_4 units such as $BC_{4-x}N_x$ is reasonable. It results from the complexation of methylamine during the synthesis of BmPSs.[17c]

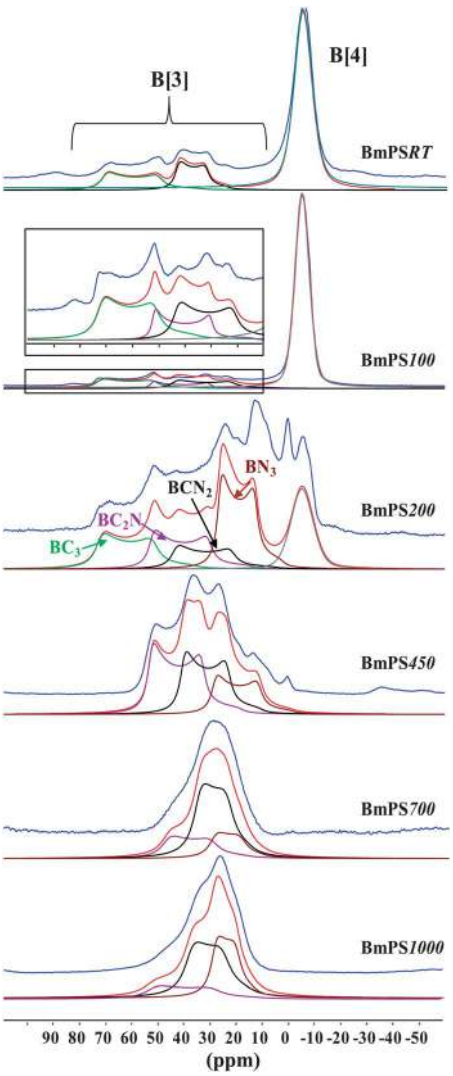

Fig. 9 ^{11}B MAS NMR experimental and simulated spectra of **BmPS*RT*** and its pyrolysis intermediates **BmPS*T* (*T*: 100 → 1000)** isolated at different temperatures.

The ^{11}B NMR spectrum of **BmPS*100*** indicates that only minor changes in the atomic structure of BmPS occur during heat treatment at 100 °C; the sharp resonance at −10 ppm points to the fact that tetra-coordinated boron units are still present in the preceramic network. After the heat-treatment at 200 °C (**BmPS*200***), the intensity of this signal is strongly reduced, whereas the intensity of resonances caused by three-fold coordinated boron atoms significantly increases. The broadness indicates a large heterogeneity in the local chemical environment of the boron nuclei and suggests the presence of tri-coordinated boron, *i.e.*, $BC_{3-x}N_x$ groups with $0 \leq x < 3$ (BC_3: $\delta_{iso}(^{11}B) = 76.5$ ppm, $C_Q = 4.2$ MHz, $\eta_Q = 0$; BC_2N: $\delta_{iso}(^{11}B) = 58.4$ ppm, $C_Q = 4.3$ MHz, $\eta_Q = 0$; BCN_2: $\delta_{iso}(^{11}B) = 45.8$ ppm, $C_Q = 4.3$ MHz, $\eta_Q = 0$; BN_3: $\delta_{iso}(^{11}B) = 30.0$ ppm, $C_Q = 3.4$ MHz, $\eta_Q = 0$). The lack of resonances in the ^{11}B NMR spectrum of **BmPS*450*** around 70 ppm and −10 ppm suggests that during the heat treatment to 450 °C, reactions at the expense of BC_3 as well as BX_4 units proceed as observed by FTIR. They are replaced by $BC_{3-x}N_x$ groups ($x = 1 \rightarrow 3$) through cleavage of the B–C bond according to eqn (10) as is commonly observed in BmPSs of the type $[B(C_2H_4SiCH_3NH)_3]_n$ and $[B(C_3H_6SiCH_3NH)_3]_n$[31,32]

$$SiC_2N_2 + BC_3 \rightarrow SiC_3N + BC_2N \qquad (10)$$

Increasing the temperature to 700 and 1000 °C (**BmPS*700*** and **BmPS*1000***) results in the formation of a mixed phase containing BCN_2 and BN_3 units in the final material.

^{29}Si CP MAS spectra of **BmPS*RT*** and its pyrolysis intermediates (**BmPS*100* → *1000***) and the ^{29}Si single pulse MAS spectrum of **BmPS*1000*** are displayed in Fig. 10.

The spectrum of **BmPS*RT*** shows a broad resonance at $\delta = 0$ ppm with a shoulder at −5 ppm.[46] These are typical values for silicon atoms in a N_2SiC_2 environment. The slight differences in the chemical shift point to the presence of cyclic $(Si–N)_x$ structures, with x-values of typically 2, 3 or 4.[46,50,51] The signal from 30 to 10 ppm is assigned to SiC_3N units in agreement with the groups usually identified in BmPSs of the type $[B(C_2H_4SiRNH)_3]_n$ (R = H, $(NH)_{0.5}$, CH_3).[8,15,31,32] This confirmed the structural rearrangement during polymer synthesis according to eqn (10).

A heat treatment at 100 and 200 °C (**BmPS*100*** and **BmPS*200***) results in a shift of the main signal toward the resonance at −5 ppm and signal sharpening. Obviously, rearrangements occur that cause a reduction of ring strains, *e.g.* by transformation of four- or eight-membered $(Si–N)_x$ ring structures ($x = 2, 4$) into thermodynamically favored six-membered rings. After calcination at 450 °C (**BmPS*450***), the proportion of SiC_3N signals around 15 ppm increases which mirrors the observation in the ^{11}B NMR spectrum, *i.e.*, an increasing proportion of BC_2N units of this sample. The strong affinity of boron to nitrogen causes B–C and Si–N bond cleavage, and formation of new B–N and Si–C bonds according to eqn (10).

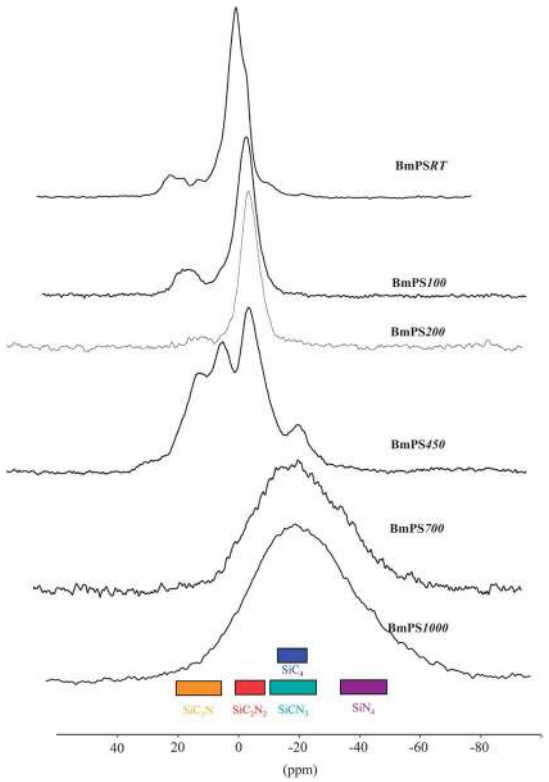

Fig. 10 ^{29}Si CP MAS NMR spectra of **BmPS*RT*** and its pyrolysis intermediates **BmPS*T* (*T*: 100 → 1000)** isolated at different temperatures. The spectrum of **BmPS*1000*** has been recorded without *cross*-polarization.

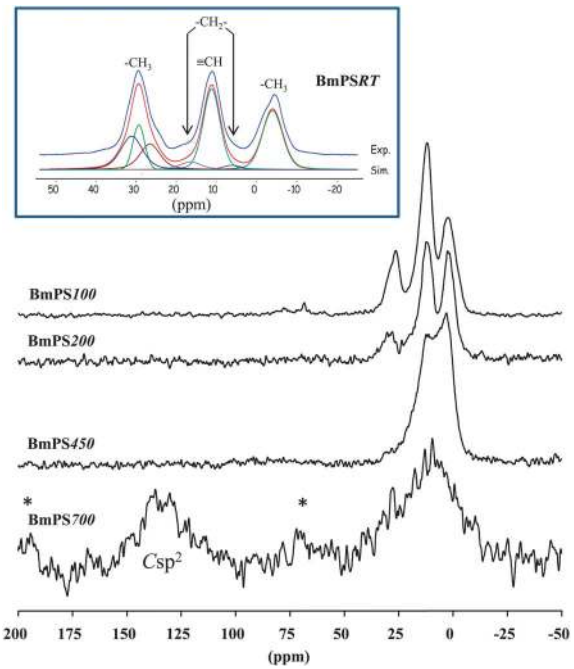

Fig. 11 ^{13}C CP MAS NMR spectra of **BmPS*RT*** and its pyrolysis intermediates **BmPS*T* (*T*: 100 → 1000)** isolated at different temperatures. A simulation is proposed for the **BmPS*RT*** spectrum.

The ^{29}Si NMR signals of the amorphous intermediates obtained after pyrolysis at 700 °C and 1000 °C (**BmPS*700*** and **BmPS*1000***) are characterized by overlapping resonances without any fine structure. They are centered at −13 ppm (**BmPS*700***) and −20 ppm (**BmPS*1000***) with a full width at half maximum of *ca.* 45 ppm and individual NMR signals arising from distinct structural units thus cannot be resolved. The appearance of such significantly broadened signals is typical for amorphous SiBCN ceramics[30–32] and it is in general caused by overlapping resonances of SiC_xN_{4-x} units with $x = 0$, 1, 2, 3 and 4. As discussed above, the FT-IR spectrum of **BmPS*700*** gave clear evidence of the presence of Si–H units. These cannot be assigned unequivocally by ^{29}Si NMR spectroscopy; however, the presence of $SiH_xC_yN_z$ units ($x + y + z = 4$) in the ^{29}Si NMR spectrum of **BmPS*700*** can neither be excluded. Furthermore, the requirement of single pulse experiments for the investigation of **BmPS*1000*** clearly points to the fact that hydrogen atoms, required for polarization transfer, are almost absent. This is in clear accordance with the IR spectrum of **BmPS*1000*** in which Si–H absorptions are not observed. Consequently, silicon atoms in **BmPS*1000*** possess mixed coordination spheres, *i.e.*, SiC_4, SiC_3N, SiC_2N_2, $SiCN_3$ and SiN_4.

The experimental ^{13}C CP MAS NMR spectra of samples **BmPS*RT*** → **BmPS*700*** are given in Fig. 11 (**BmPS*1000*** could not be recorded with CP due to the absence of protons). The ^{13}C NMR spectrum of **BmPS*RT*** exhibits three main signals at −3 ppm with a shoulder at 0 ppm, 11 ppm and 30 ppm with a shoulder at 25 ppm. Using the Inversion Recovery Cross Polarization (IRCP) technique in which the dynamics of polarization inversion depend on the proton environment,[52–54] the spectrum could be simulated with seven signals: *(i)* two signals around 6 and 17 ppm were assigned to $-CH_2-$ units; *(ii)* one signal at 11 ppm has been attributed to CH groups; and (iii) the remaining resonance signals at −3, 27, 30 and 31 ppm have been assigned to CH_3 environments exhibiting a weak $^{13}C-^{1}H$ dipolar coupling due to their mobility.[17c,55]

The signal appearing at −3 ppm corresponds to Si*C*H$_3$. The assignment of resonances caused by the C_2H_4 group is complex. Since the hydroboration of $H_3CSiCl_2(HC{=}CH_2)$ is not regioselective, both the α-addition product with the Si–HC(CH$_3$)–B moiety and the β-addition product with the Si–CH$_2$–CH$_2$-B unit form. The α:β ratio in general depends on the substitution pattern on silicon; for $H_3CSiCl_2(HC{=}CH_2)$ and the use of borane dimethylsulfide as the hydroboration reagent, it is 2 : 1. Typical ^{13}C chemical shift values of Si*C*HCH$_3$B and SiCH*C*H$_3$B are 10–15 ppm and 16–25 ppm,[30–32] respectively, and correspond to the signals observed at 11 and 27 ppm in good agreement with the degree of protonation extracted from IRCP experiments. Resonances of Si*C*H$_2$CH$_2$B and SiCH$_2$*C*H$_2$B carbon atoms usually appear at 0–8 ppm and 15–19 ppm.[30–32] CH_2- resonances observed around 6 and 17 ppm were therefore assigned to Si*C*H$_2$CH$_2$B and SiCH$_2$*C*H$_2$B moieties, respectively. Finally, resonance signals observed at ∼30 ppm were attributed to the carbon element in N*C*H$_3$ groups.

The main structural changes during the cross-linking of **BmPS*RT*** in an ammonia atmosphere are caused by trans-amination, *i.e.*, replacement of $NCH_3/NHCH_3$ with NH_2 groups and their subsequent condensation. Consequently, the relative intensity of the N*C*H$_3$ signal in the spectrum of **BmPS*100*** decreases in comparison with that of **BmPS*RT***. As evident from

the ^{29}Si NMR data, reaction of Si*C*H$_3$ groups which are still present with the ammonia treatment is limited. However, the substitution of NCH$_3$ with NH units results in a broadening of the Si*C*H$_3$ signal and a slight shift to a lower field, *i.e.*, from −5 to 0 ppm. The ^{13}C NMR spectrum of **BmPS*200*** is more or less identical to that one recorded for **BmPS*100***; it merely displays a N*C*H$_3$ resonance signal which further decreases in intensity and finally disappears after the heat treatment at 450 °C (**BmPS*450***).

The spectrum of **BmPS*700*** shows a significantly broadened ^{13}C NMR signal in the aliphatic region that can be assigned to CH$_x$Si$_{4-x}$ units (with x = 0, 1, 2).[30–32] The drastically reduced signal to noise ratio reflects the transformation of the BmPSs into an amorphous network, which is in good agreement with TG experiments shown above. In addition, a broad signal in the low-field region appears in the range of 130–140 ppm, indicating the formation of amorphous (graphite-like) carbon during the thermal degradation.[56,57]

The individual decomposition steps occurring during thermolysis of [B(C$_2$H$_4$SiCH$_3$NCH$_3$)$_3$]$_n$ suggested by the results of TGA, IR and NMR investigations are outlined in Scheme 1.

Based on its chemical composition ([Si$_{3.0}$B$_{1.1}$C$_{11.8}$N$_{3.6}$H$_{37.7}$]$_n$), molecular weight (631.5 g mol^{-1}, determined by Maldi-Tof spectrometry) and compositional units identified by IR and solid-state NMR spectroscopies, we tentatively propose the following structure of **BmPS*RT***. It is composed of 6- and 4-membered (–Si–N–)$_n$ rings which are cross-linked by BX$_3$ groups including BC$_3$ and, to a minor extent BC$_2$N and/or BCN$_2$ as well as BX$_4$ units, *i.e.*, BC$_{4-x}$N$_x$ units. Terminal N(H)CH$_3$ groups are also identified.

A precise determination of the local environment of the tri-coordinated boron atoms linked to nitrogen (BC$_2$N and BCN$_2$) is not possible. Within this context, we decided to introduce BCN$_2$ groups keeping in mind that the reader should not conclude that the structure depicted in Scheme 1 is necessarily the real one. Some structural variations can appear but the proposed structure is the one which represents the best compromise among chemical composition, molecular weight and solid-state NMR results.

Initially, cross-linking reactions occur at low temperatures in an ammonia atmosphere. Both internal N–CH$_3$ groups and terminal NHCH$_3$ groups are replaced with NH and/or NH$_2$ units through trans-amination reactions. In this temperature range, the local structure of the boron atoms, *i.e.*, the four-fold coordination changes toward three-fold coordination. At intermediate temperatures, ammonia and hydrocarbons are the main gaseous by-products, as identified by GCMS, suggesting the appearance of condensation reactions by releasing ammonia and the cleavage of Si–C, B–C, C–C and C–H bonds with formation of C and H radicals, resulting in the elimination of low molecular weight hydrocarbons. In the high temperature regime of the thermal decomposition, the remaining hydrogen atoms linked to Si and N are gradually removed as molecular hydrogen in dehydrocoupling reactions leading to the formation of Si–N bonds. The material produced at 1000 °C (**BmPS*1000***) presents an amorphous network as identified by X-ray diffraction (*see* ESI, Fig. S3†) composed of silicon, boron, carbon and nitrogen in which (*i*) boron atoms have BCN$_2$ and BN$_3$ coordinations, (*ii*) silicon atoms are mainly bonded to nitrogen and carbon possessing a local SiC$_x$N$_{4-x}$ (x = 0, → 4) environment as well as (*iii*) graphite-like carbon domains. However, it should be mentioned that a finite amount of hydrogen at or near the phase boundaries of remaining amorphous carbon can be detected by ^{1}H solid-state NMR investigation of SiBCN materials prepared from BmPSs of the type [B(C$_3$H$_6$SiCH$_3$NH)$_3$]$_n$ after exposures at 2000 °C.[31] In our samples prepared at 1000 °C, we based our comment concerning the absence of hydrogen on FT-IR and ^{13}C, ^{11}B, ^{29}Si NMR investigations. Further investigations are therefore required to precisely determine residual hydrogen in the samples described here.

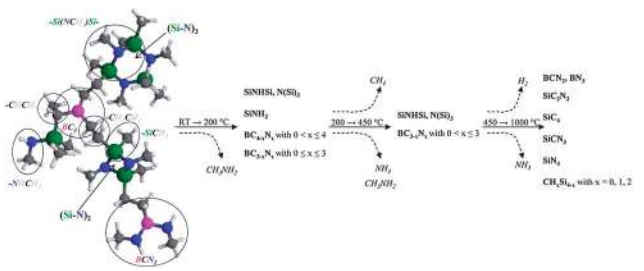

Scheme 1 Experimentally observed chemical pathways in the pyrolytic decomposition of **BmPS*RT*** to amorphous SiBCN ceramics.

4 Conclusions

The thermal transformation of BmPSs of the type [B(C$_2$H$_4$SiCH$_3$NCH$_3$)$_3$]$_n$ (C$_2$H$_4$ = CHCH$_3$, CH$_2$CH$_2$) into an amorphous SiBCN ceramic was studied by a combination of *in situ* thermo-analytical experiments such as TGA–DTG coupled with mass spectroscopy/gas chromatography and *ex situ* solid-state ^{11}B, ^{13}C, ^{29}Si MAS NMR investigations as well as IR spectroscopy. The results yielded new insights into the degradation mechanisms occurring during the thermal decomposition of SiBCN precursors between room temperature and 1000 °C. Thermolysis, which was performed in NH$_3$ up to 200 °C and in N$_2$ between 200 and 1000 °C yielded an amorphous ceramic which possessed h-BN or BCN, SiC$_x$N$_{4-x}$ (x = 0, → 4) and graphite domains.

The ceramic conversion under ammonia starts with evolution of methylamine *via* trans-amination and transformation of BC$_3$ and BC$_3$N into BC$_{3-x}$N$_x$ units with x = 1–3. It is followed by evolution of hydrocarbons due to the cleavage of B–C, Si–C, and Si–H bonds and formation of radicals that abstract hydrogen. In the high temperature regime of the pyrolytic degradation dehydrocoupling reactions take place, which result in the elimination of molecular hydrogen. It is observed that the transformation of processable BmPSs into an amorphous ceramic network is almost completed at ~700 °C. From the present point of view, further heating to 1000 °C causes only minor changes in both composition and atomic structure, which cannot be determined in detail experimentally by the methods we applied. [B(C$_2$H$_4$SiCH$_3$NCH$_3$)$_3$]$_n$ possesses proper rheology and viscosity to be melt spun into green fibers. Thermolysis in ammonia atmosphere at 200 °C is a very suitable and cheap means to surface-harden the fibers in order to maintain their shape during a subsequent heat treatment. Such ceramization up to 1000 °C (or even 1400 °C) in a nitrogen atmosphere releases amorphous SiBCN ceramic fibers which possess excellent thermo-mechanical properties, as will be published soon. These findings clearly point

to the fact that the design of the intermediate pyrolysis steps of $[B(C_2H_4SiCH_3NCH_3)_3]_n$ by carefully choosing proper conditions for its polymer-to-ceramic conversion is of major importance to convert the polymeric precursor into high-performance amorphous SiBCN ceramics.

Acknowledgements

We thank the European Community who supported this work through the Marie Curie Research Training Network PolyCerNet (Contract MRTN-CT-2005-019601). The authors wish to thank François Toche and Rodica Chiriac for their contribution to GC/MS as well as Kathrin Inzenhofer and Günter Motz for the investigation of the Maldi-Tof spectrometry.

Notes and references

1 J. Bill and F. Aldinger, *Adv. Mater.*, 1995, **7**, 775.
2 R. Riedel, G. Mera, R. Hauser and A. Klonczynski, *J. Ceram. Soc. Jpn.*, 2006, **114**, 425.
3 *Polymer Derived Ceramics: Theory and Applications*, by ed. P. Colombo, G. D. Soraru, R. Riedel, A. Kleebe, DEStech Publications, Inc., 2009.
4 P. Colombo, G. Mera, R. Riedel and G. D. Soraru, *J. Am. Ceram. Soc.*, 2010, **93**, 1805.
5 J. G. Alauzun, S. Ungureanu, N. Brun, S. Bernard, P. Miele, R. Backov and C. Sanchez, *J. Mater. Chem.*, 2011, **21**, 14025.
6 M. Zaheer, T. Schmalz, G. Motz and R. Kempe, *Chem. Soc. Rev.*, 2012, **41**, 5102.
7 E. Ionescu, H.-J. Kleebe and R. Riedel, *Chem. Soc. Rev.*, 2012, **41**, 5032.
8 R. Riedel, A. Kienzle, W. Dressler, L. Ruwisch, J. Bill and F. Aldinger, *Nature*, 1996, **382**, 796.
9 T. Wideman, E. Cortez, E. E. Remsen, G. A. Zank, P. J. Carrol and L. G. Sneddon, *Chem. Mater.*, 1997, **9**, 2218.
10 D. Srivastava, E. N. Duesler and R. T. Paine, *Eur. J. Inorg. Chem.*, 1998, **1998**, 855.
11 F. Aldinger, M. Weinmann and J. Bill, *Pure Appl. Chem.*, 1998, **70**, 439.
12 M. Weinmann, R. Haug, J. Bill, M. De Guire and F. Aldinger, *Appl. Organomet. Chem.*, 1998, **12**, 725.
13 H. P. Baldus, M. Jansen and D. Sporn, *Science*, 1999, **285**, 699.
14 M. Weinmann, T. W. Kamphowe, J. Schuhmacher, K. Müller and F. Aldinger, *Chem. Mater.*, 2000, **12**, 2112.
15 M. Weinmann, J. Schuhmacher, H. Kummer, S. Prinz, J. Peng, H. J. Seifert, M. Christ, K. Müller, J. Bill and F. Aldinger, *Chem. Mater.*, 2000, **12**, 623.
16 Z.-C. Wang, F. Aldinger and R. Riedel, *J. Am. Ceram. Soc.*, 2001, **84**, 2179.
17 (*a*) S. Bernard, M. Weinmann, D. Cornu, P. Miele and F. Aldinger, *J. Eur. Ceram. Soc.*, 2005, **25**, 251; (*b*) S. Bernard, M. Weinmann, P. Gerstel, P. Miele and F. Aldinger, *J. Mater. Chem.*, 2005, **5**, 289; (*c*) L. Gottardo, S. Bernard, C. Gervais, K. Inzenhofer, G. Motz, M. Weinmann, C. Balan and P. Miele, *J. Mater. Chem.*, 2012, **22**, 7739.
18 R. Hauser, S.-N. Borchard, R. Riedel, Y. H. Ikuhara and Y. Iwamoto, *J. Ceram. Soc. Jpn.*, 2006, **114**, 524.
19 (*a*) P. Miele, S. Bernard, D. Cornu and B. Toury, *Soft Mater*, 2006, **4**, 249; (*b*) S. Bernard, S. Duperrier, D. Cornu, P. Miele, M. Weinmann, C. Balan and F. Aldinger, *J. Optoelectron.Adv. Mater.*, 2006, **8**, 648.
20 X. B. Yan, P. Dibandjo, S. Bernard, L. Gottardo, H. Mouttaabidd and P. Miele, *Chem. Mater.*, 2008, **20**, 6325.
21 L. Gottardo, S. Bernard, M.-P. Berthet and P. Miele, *Key Eng. Mater.*, 2008, **368-372**, 926.
22 U. Müller, M. Weinmann and M. Jansen, *J. Mater. Chem.*, 2008, **18**, 3671.
23 S. Sarkar, Z. Gan, L. An and L. Zhai, *J. Phys. Chem. C*, 2011, **115**, 24993.
24 O. Majoulet, J. G. Alauzun, L. Gottardo, C. Gervais, M. E. Schuster, S. Bernard and P. Miele, *Microporous Mesoporous Mater.*, 2011, **140**, 40.
25 J. Wilfert, R. Von Hagen, R. Fiz, M. Jansen and S. Mathur, *J. Mater. Chem.*, 2012, **22**, 2099.
26 N. Janakiraman, M. Weinmann, J. Schuhmacher, K. Müller, J. Bill, F. Aldinger and P. Singh, *J. Am. Ceram. Soc.*, 2002, **85**, 1807.
27 R. N. V. Kumar, S. Prinz, Y. Cai, A. Zimmermann, F. Aldinger, F. Berger and K. Müller, *Acta Mater.*, 2005, **53**, 4567.
28 (*a*) S. Duperrier, S. Bernard, A. Calin, C. Sigala, R. Chiriac, P. Miele and C. Balan, *Macromolecules*, 2007, **40**, 1028; (*b*) S. Duperrier, A. Calin, S. Bernard, C. Balan and P. Miele, *Soft Mater.*, 2006, **2**, 123.
29 M. Gunthner, T. Kraus, A. Dierdorf, D. Decker, W. Krenkel and G. Motz, *J. Eur. Ceram. Soc.*, 2009, **29**, 2061.
30 G. Schumacher, F. Berger, M. Weinmann, J. Bill, F. Aldinger and K. Muller, *Appl. Organomet. Chem.*, 2001, **15**, 809.
31 F. Berger, A. Müller, F. Aldinger and K. Müller, *Z. Anorg. Allg. Chem.*, 2005, **631**, 355.
32 C. Gervais, F. Babonneau, L. Ruwisch, R. Hauser and R. Riedel, *Can. J. Chem.*, 2003, **81**, 1.
33 (*a*) S. Duperrier, C. Gervais, S. Bernard, D. Cornu, F. Babonneau and P. Miele, *J. Mater. Chem.*, 2006, **16**, 3126; (*b*) S. Bernard, K. Fiaty, D. Cornu, P. Miele and P. Laurent, *J. Phys. Chem. B*, 2006, **110**, 9048.
34 D. Massiot, F. Fayon, M. Capron, I. King, S. Le Calvé, B. Alonso, J.-O. Durand, B. Bujoli, Z. Gan and G. Hoatson, *Magn. Reson. Chem.*, 2002, **40**, 70.
35 R. Jones and J. K. Myers, *J. Organomet. Chem.*, 1972, **34**, C9.
36 M. Weinmann, T. W. Kamphowe, P. Fischer and F. Aldinger, *J. Organomet. Chem.*, 1999, **592**, 115.
37 J. Schuhmacher, Ph. D. thesis, Univ. Stuttgart2000.
38 N. S. Choong Kwet Yive, R. J. P. Corriu, D. Leclercq, P. H. Mutin and A. Vioux, *Chem. Mater.*, 1992, **4**, 141.
39 Z. Xie, S. Cao, J. Wang, X. B. Yan, S. Bernard and P. Miele, *Mater. Sci. Eng.*, 2010, **527**, 7086.
40 S. Kokott and G. Motz, *Soft Mater.*, 2006, **4**, 165.
41 (*a*) S. Duperrier, R. Chiriac, C. Sigala, C. Gervais, S. Bernard, D. Cornu and P. Miele, *J. Eur. Ceram. Soc.*, 2009, **29**, 851; (*b*) P. Toutois, P. Miele, S. Jacques, D. Cornu and S. Bernard, *J. Am. Ceram. Soc.*, 2006, **89**, 42.
42 W. R. Schmidt, P. S. Marchetti, L. V. Interrante, W. J. Hurley Jr, R. H. Lewis, R. H. Doremus and G. E. Maciel, *Chem. Mater.*, 1992, **4**, 937.
43 N. S. Choong Kwet Yive, R. J. P. Corriu, D. Leclercq, P. H. Mutin and A. Vioux, *Chem. Mater.*, 1992, **4**, 1263.
44 R. M. Laine and F. Babonneau, *Chem. Mater.*, 1993, **5**, 60.
45 S. Trafl, D. Suttor, G. Motz, E. Rossler and G. Ziegler, *J. Eur. Ceram. Soc.*, 2000, **20**, 215.
46 J. Seitz, J. Bill, N. Egger and F. Aldinger, *J. Eur. Ceram. Soc.*, 1996, **16**, 885.
47 (*a*) G. Jeschke, M. Kroschel and M. Jansen, *J. Non-Cryst. Solids*, 1999, **260**, 216; (*b*) Y. H. Sehlleier, A. Verhoeven and M. Jansen, *J. Mater. Chem.*, 2007, **17**, 4316; (*c*) Y. H. Sehlleier, A. Verhoeven and M. Jansen, *Angew. Chem., Int. Ed.*, 2008, **47**, 3600.
48 (*a*) S. Duperrier, C. Gervais, S. Bernard, D. Cornu, F. Babonneau, C. Balan and P. Miele, *Macromolecules*, 2007, **40**, 1018; (*b*) J. Li, V. Salles, S. Bernard, C. Gervais and P. Miele, *Chem. Mater.*, 2010, **22**, 2010; (*c*) S. Schlienger, J. Alauzun, F. Michaux, L. Vidal, J. Parmentier, C. Gervais, F. Babonneau, S. Bernard, P. Miele and J. B. Parra, *Chem. Mater.*, 2012, **24**, 88.
49 W. R. Schmidt, D. M. Narsavage-Heald, P. S. Jones, Marchetti, D. Raker and G. E. Maciel, *Chem. Mater.*, 1999, **11**, 1455.
50 N. S. Choong Kwet Yive, R. J. P. Corriu, D. Leclercq, P. H. Mutin and A. Vioux, *New J. Chem.*, 1991, **15**, 85.
51 C. Gerardin, F. Taulelle and J. Livage, *Mater. Res. Soc. Symp. Proc.*, 1993, **287**, 233.
52 X. Wu and K. W. Zilm, *J. Magn. Reson.*, 1993, **102**, 205.
53 P. Palmas, P. Tekely and D. Canet, *J. Magn. Reson., Ser. A*, 1993, **104**, 26.
54 R. Sangill, N. Rastrup-Andersen, H. Bildsoe, H. J. Jakobsen and N. C. Nielsen, *J. Magn. Reson.*, 1994, **107**, 67.
55 L. B. Alemany, D. M. Grant, R. J. Pugmire, T. D. Alger and K. W. Zilm, *J. Am. Chem. Soc.*, 1983, **105**, 2133.
56 J. Schuhmacher, M. Weinmann, J. Bill, F. Aldinger and K. Müller, *Chem. Mater.*, 1998, **10**, 3913.
57 K. Müller, in *Grain Boundary Dynamics of Precursor-Derived Covalent Ceramics*, ed. J. Bill, F. Wakai, F. Aldinger; Wiley-VCH, Weinheim, 1999, p. 197.